https://doi.org/10.5194/tc-2021-327
Preprint. Discussion started: 19 October 2021


The Cryosphere Discussions

# Shear-margin melting causes stronger transient ice discharge than ice-stream melting according to idealized simulations

Johannes Feldmann[1], Ronja Reese[1,2], Ricarda Winkelmann[1,3], and Anders Levermann[1,3,4]

[1]Potsdam Institute for Climate Impact Research (PIK), Potsdam, Germany
[2]Department of Geography and Environmental Sciences, Northumbria University, Newcastle, UK
[3]Institute of Physics, University of Potsdam, Potsdam, Germany
[4]LDEO, Columbia University, New York, USA

*Correspondence to:* Johannes Feldmann (johannes.feldmann@pik-potsdam.de)

**Abstract.** Basal ice-shelf melting is the key driver of Antarctica's increasing sea-level contribution. In diminishing the buttressing force of the ice shelves that fringe the ice sheet the melting increases the solid-ice discharge into the ocean. Here we contrast the influence of basal melting in two different ice-shelf regions on the time-dependent response of an idealized, inherently buttressed ice-sheet-shelf system. Carrying out three-dimensional numerical simulations, the basal-melt perturbations are applied close to the grounding line in the ice-shelf's 1) ice-stream region, where the ice shelf is fed by the fastest ice masses that stream through the upstream bed trough and 2) shear margins, where the ice flow is slower. The results show that melting below one or both of the shear margins can cause a decadal to centennial increase in ice discharge that is more than twice as large compared to a similar perturbation in the ice-stream region. We attribute this to the fact that melt-induced ice-shelf thinning in the central grounding-line region is attenuated very effectively by the fast flow of the central ice stream. In contrast, the much slower ice dynamics in the lateral shear margins of the ice shelf facilitate sustained ice-shelf thinning and thereby foster buttressing reduction. Regardless of the melt location, a higher melt concentration toward the grounding line generally goes along with a stronger response. Our results highlight the vulnerability of outlet glaciers to basal melting in stagnant, buttressing-relevant ice-shelf regions, a mechanism that may gain importance under future global warming.

## 1 Introduction

Virtually all of Antarctica's observed sea-level contribution comes from increased discharge of solid ice into the ocean (Rignot et al., 2019; The IMBIE Team, 2020). The discharge is regulated by the floating ice shelves that fringe the ice sheet and exert a buttressing force on the upstream outlet glaciers that drain the ice sheet (Dupont and Alley, 2005; Schoof, 2007; Goldberg et al., 2009; Favier et al., 2012; Gudmundsson et al., 2012; Haseloff and Sergienko, 2018; Pegler, 2018; Reese et al., 2018). Basal melting and thus thinning of buttressing ice shelves (Rignot et al., 2013; Paolo et al., 2015) reduces their backforce which can lead to speed-up, thinning and retreat of the upstream grounded masses (Shepherd et al., 2002; Jenkins et al., 2010; Joughin and Alley, 2011; Rignot et al., 2014; Konrad et al., 2018).

Future atmospheric warming will likely increase the oceanic heat content available for sub-ice-shelf melting (Rignot and Jacobs, 2002; Hellmer et al., 2012; Spence et al., 2014; Schmidtko et al., 2014; Naughten et al., 2018). Increased melting may

https://doi.org/10.5194/tc-2021-327
Preprint. Discussion started: 19 October 2021


lead to increased ice discharge and thus contribute positively to future sea level rise (e.g., Bindschadler et al., 2013; Bamber and Aspinall, 2013; Joughin et al., 2014; Favier et al., 2014; Mengel and Levermann, 2014; Pollard et al., 2015; Bakker et al., 2017; Jackson et al., 2018; Levermann et al., 2020; Payne et al., 2021; Edwards et al., 2021).

Observations of Antarctic outlet glaciers show that sub-ice-shelf melt rates are typically strongest close to the grounding line where fast and thick ice masses cross the outlets' central grounding-line section (Dutrieux et al., 2013; Shean et al., 2019). However, ice-shelf melting as well as thinning patterns can be spatially very heterogeneous (Pritchard et al., 2012; Dutrieux et al., 2013; Paolo et al., 2015), including the possibility of comparatively strong melting in the more stagnant parts of an ice shelf, e.g., regions at the lateral margins of the fast-flowing ice streams or regions close to ice rises (Berger et al., 2017; Goldberg et al., 2019; Shean et al., 2019; Adusumilli et al., 2020).

Gagliardini et al. (2010) found in conceptual flowline simulations that the grounding-line position and the volume of an ice sheet are sensitive to changes in the degree of concentration of the melting to the grounding line even if the average melt magnitude remains the same. This suggests that not only the magnitude but also the location and distribution of ice-shelf thinning have strong influence on the backstress and the corresponding ice-sheet response. Reese et al. (2018) conducted diagnostic perturbation experiments to assess the instantaneous response of the integrated flux across the grounding line of the Antarctic Ice Sheet to local melt perturbations of its ice shelves. Their results indicate that in general perturbations closer to the grounding lines induced stronger responses. Strongest flux responses were induced in regions close to the grounding lines of ice streams but high responses were also found in regions close to pinning points or shear margins. Zhang et al. (2020) used the same perturbation method and compared it to an adjoint-based approach which allows for higher spatial resolution. They applied both approaches in an idealized setup and a real-world setup of Larsen C, showing their consistency and finding also that the integrated grounding-line flux is most sensitive to ice-shelf thinning close to the grounding line. Using the adjoint-based method in prognostic simulations of Crosson and Dotson ice shelves and their feeding glaciers in West Antarctica, Goldberg et al. (2019) found that the linearized response of the glaciers' sea-level relevant ice volume over 15 years is, consistently with the instantaneous studies by Reese et al. (2018) and Zhang et al. (2020), most sensitive to ice-shelf melting close to the grounding lines and regions of high horizontal shearing.

Here we carry out transient, three-dimensional, idealized numerical simulations to compare the effects of basal melting in the central ice-stream region vs. the lateral shear-margin regions within an ice-shelf embayment that buttresses an upstream outlet glacier. That is, simulating an inherently buttressed ice-sheet-shelf system we examine its time-dependent response to the perturbations with respect to changes in ice geometry, buttressing, ice discharge and grounding-line position. This is done over a time period of 100 years that is longer than previous studies. Besides altering the melt location (beneath the ice-stream / beneath one or both shear-margins) we also vary the magnitude and the spatial extent of the perturbation. The numerical model and the experimental design are outlined in Sec. 2. The results are analyzed in Sec. 3 and discussed in Sec. 4 where we also conclude.

https://doi.org/10.5194/tc-2021-327
Preprint. Discussion started: 19 October 2021


The Cryosphere Discussions

## 2 Methods

### 2.1 Numerical model

We use the open-source Parallel Ice Sheet Model (PISM; Bueler and Brown, 2009; Winkelmann et al., 2011; Khroulev and Authors, 2020), version stable1.0 (https://github.com/pism/pism/). The model applies a superposition of the shallow-ice approximation (SIA; Morland, 1987) and the shallow-shelf approximation (SSA; Hutter, 1983) of the Stokes stress balance (Greve and Blatter, 2009). In particular, the SSA allows for stress transmission across the grounding line and thus accounts for the buttressing effect of laterally confined ice shelves on the upstream grounded regions (Gudmundsson et al., 2012; Fürst et al., 2016; Reese et al., 2018). The model applies a linear interpolation of the freely evolving grounding line and accordingly interpolated basal friction (Feldmann et al., 2014). Grounding-line migration has been evaluated in the model intercomparison exercises MISMIP3d (Pattyn et al., 2013; Feldmann et al., 2014) and MISMIP+ (Asay-Davis et al., 2016; Cornford et al., 2020). To improve the approximation of driving stress across the grounding line, the surface gradient is calculated using centered differences of the ice thickness across the grounding line (Reese et al., 2020).

### 2.2 Setup and experimental design

The model is initiated with a block of ice from which the ice-sheet-shelf system evolves, reaching equilibrium after several 1,000 model years. The prescribed surface mass balance and ice softness are constant in space and time (see Table 1 for more parameters). Basal friction is calculated according to a Weertman-type power law (Asay-Davis et al., 2016, Eq. 6). The prescribed bed topography is taken from MISMIP+ (Asay-Davis et al., 2016, Eq. 1) which is a smaller version of the one from Gudmundsson et al. (2012). It is designed to model an idealized, strongly buttressed, marine ice sheet, which is drained by an ice stream through a bed trough, feeding a bay-shaped ice shelf which calves into the ocean (Figs. 1, 2 and A1). The bed topography is a superposition of two components: the bed elevation in $x$-direction is overall declining from the ice divide towards the ocean but has an overdeepening (landward down-sloping bed section) just upstream of the continental shelf break. The bed component in $y$-direction has a channel-shaped form. The superposition of both components yields a bed trough which is symmetric in the $y$-direction (symmetry axis $y = 0$). While the main ice flow is in $x$-direction (from the interior through the bed trough towards the ocean) there is also a flow component in $y$-direction, i.e., from the channel's lateral ridges down into the trough. Resulting convergent flow and associated horizontal shearing enable the emergence of buttressing. Ice is cutoff from the ice shelf and thus calved into the ocean beyond a fixed position $x_{\mathrm{cf}} = 640\ \mathrm{km}$. During the model spinup no sub-ice-shelf melting is applied. The simulations are carried out using a horizontal resolution of $1\ \mathrm{km}$.

While the model spinup is closely along the lines of the MISMIP+ experiments, the design of the perturbation experiments is different in this study. Starting from the steady-state ice-sheet-shelf system, basal melting is introduced close to the grounding line in either the central ice-stream region or the lateral shear-margin region(s) of the ice shelf. Ice-stream melting (IS) is confined to the center of the ice shelf, where the ice stream crosses the grounding line (Fig. 3). Shear-margin melting is applied to one (SM1) or both (SM2) of the two shear margins of the ice-shelf bay, where the ice flows from the ridges into the ice shelf. In each of the three experiments IS, SM1 and SM2 the melt perturbation is applied over an area of the same length

https://doi.org/10.5194/tc-2021-327
Preprint. Discussion started: 19 October 2021


The Cryosphere Discussions

$l = 21$ km along the grounding line. The width $w$, i.e., the extent of the perturbation area into the ice shelf (in $x$-direction for IS and in $y$-direction for SM1/SM2, respectively) is varied between 2 and 16 km in different simulations. This allows us to compare between very confined (small $w$) and more distributed (large $w$) melt patterns while keeping the total sub-shelf mass flux rate $P$ constant. In a further set of experiments $P$ is varied between 0.5 and 2 Gt/yr to investigate the influence of the total melt magnitude. Throughout all experiments, the resulting local melt rates range between $\approx 6$ m/yr ($P = 0.5$ Gt/yr, $w = 16$ km) and $\approx 52$ m/yr ($P = 2$ Gt/yr, $w = 2$ km). The location of the melt area is determined at each model time step and hence adapts to grounding-line movement. It excludes the first floating grid cells directly downstream of the grounding line to assure that the driving stress upstream of the grounding line is not changed by the perturbations. In the IS experiments the location of the perturbation area is symmetric with respect to the setup centerline. In the SM1/SM2 experiments, the $x$-location of the perturbation area also adapts to the length of the confined part of the ice shelf, which we calculate from the $x$-location of the grounding line at the center ($y = 0$ km), $x_{c0}$, and at the margins ($y = \pm 40$ km), $x_{c1}$, of the channel setup. The center of the perturbation area is placed at $x = x_{c0} + 0.4(x_{c1} - x_{c0})$ and thus slightly upstream of the half length of the ice-shelf confinement to exclude melting near "fangs" – grounded features between 480 and 510 km in steady state (Asay-Davis et al., 2016; Cornford et al., 2020). The simulations are run for 100 model years. An unperturbed control run is carried out serving as the reference for the calculation of the time-dependent anomalies.

### 2.3 Cumulative flux response number

Based on buttressing flux response number $\theta_B$ from Reese et al. (2018) we here define the cumulative flux response number (cFRN) as the ratio of the time-integrated change in grounding-line flux and the applied perturbation rate, respectively:

$$\mathrm{cFRN}(t) = \frac{\int_0^t R(t')dt'}{\int_0^t P dt'}, \tag{1}$$

where $R$ is the flux change integrated over the entire grounding line with respect to the reference run and $P$ the perturbation strength (applied total basal melt rate). The cFRN provides a cumulative measure of the sea-level relevant ice-sheet response that is normalized to the applied perturbation magnitude. In a way, the cFRN measures the efficiency of the melting, i.e., a larger value of the cFRN means that the same perturbation magnitude causes more grounded mass loss. If its value would be one, then the cumulatively perturbed ice mass translates into the same amount of grounding-line flux increase and thus grounded ice loss. A value of zero would occur in an unbuttressed situation, where melting of the ice shelf does not affect the grounding-line flux at all.

## 3 Results

The spun-up ice-sheet-shelf system is characterized by a fast, $\sim 50$ km wide, ice stream that accelerates towards the ice shelf, being sharply confined by the lateral bed topography (Figs. 1-2). The strong buttressing force of the ice shelf inside the confinement allows for a stable central grounding-line position on the retrograde slope section (Fig. 1).

https://doi.org/10.5194/tc-2021-327
Preprint. Discussion started: 19 October 2021


The Cryosphere Discussions
Open Access
EGU

In the perturbation experiments the buttressing is reduced as the applied sub-ice-shelf-melting thins the ice shelf locally. This causes an increase in ice discharge across the grounding line (Fig. 4), accompanied by speed-up and thinning of the grounded portion of the ice sheet, inducing grounding-line retreat (Figs. 5, 6). These effects occur regardless of the location of the perturbations applied in this study. However, the magnitude of the ice-sheet response differs between the three types of experiments, as shown by the cFRN.

Comparing experiments IS and SM2 for the same applied perturbation magnitude (total basal melt rate $P = 2$ Gt/yr), the response to the SM2 perturbation is generally stronger in terms of ice-flux increase across the grounding line, ice-flow acceleration, ice thinning and grounding-line retreat (Figs. 4-6). Though the SM2 perturbation removes the same amount of mass from the ice shelf the induced loss in grounded ice mass, i.e., the sea-level contribution, is about twice as large compared to the IS case. Applying the lateral melt perturbation at only one side of the ice shelf (experiment SM1) with a total melt rate of $P = 1$ Gt/yr can also be thought of as masking out one of the two melt areas in the SM2 experiment. This perturbation leads to grounded-ice acceleration and grounding-line retreat similar to the IS case, thus being weaker than in the SM2 case. However, relative to the applied perturbation strength the response magnitude is twice as large compared to the IS experiments and on the same order of the SM2 experiments, as can be seen from the cFRN (Fig. 4). In other words, melting at (one of) the ice-shelf shear margins (SM1/SM2) is twice as effective compared to ice-stream melting (IS) as it requires only half of the perturbation strength to induce the same response magnitude.

The primary reason for the different ice-sheet response magnitudes to the ice-stream and shear-margin perturbations, respectively, lies in the finding that basal melting in the shear-margin regions has a more sustained effect on local ice-shelf thinning, implying a stronger reduction in ice-shelf buttressing (Fig. A2). As can be seen from Fig. 5, the local reduction of the ice-shelf thickness in the shear-margin case can be twice as large as in the ice-stream case. This is due to the fact that the ice supply from the lateral ridges (where the ice is very stagnant) into the lateral perturbation areas is comparatively low (Fig. A1). In contrast, inside the bed trough there is strong ice advection from the ice-sheet interior towards the grounding-line. This advection counteracts ice-shelf thinning most efficiently in the center of the trough, where the ice stream is fastest (compare ice-shelf thinning patterns in Fig. 5). The strong decline of the ice stream's speed/flux towards the trough's margins limits its ability to dampen lateral ice-shelf thinning. Furthermore, while almost the entire ice shelf accelerates in the SM1/SM2 experiments (local speed-up of over $100\mathrm{m/yr}$), in the IS experiment the major ice-shelf part downstream of the perturbation area slightly decelerates (Fig. 6) due to the thinning-induced weakening of the driving stress in main flow ($x-$) direction. This leads to reduced advection out of the central perturbation area, providing additional attenuation of the thinning there. At the same time, this advection is large enough to effectively smear out the thinning signal in downstream direction (Fig. 5), where it has less effect on buttressing (Reese et al., 2018).

Above we saw for an exemplary perturbation strength of $P = 2$ Gt/yr that shear-margin melting can be twice as efficient as ice-stream melting (Fig. 4). To quantify the difference in the response magnitude for all ice-stream and shear-margin melt perturbations, respectively, we calculate the ratio of the cFRN values, i.e., $r_{\mathrm{SM1}} = \frac{\mathrm{cFRN_{SM1}}}{\mathrm{cFRN_{IS}}}$ and $r_{\mathrm{SM2}} = \frac{\mathrm{cFRN_{SM2}}}{\mathrm{cFRN_{IS}}}$. For the major part of the perturbation period, shear-margin melt induces a stronger response than ice-stream melt (exception: $w = 16$ km, $P = 0.5$ Gt/yr) and it thus holds $r_{\mathrm{SM1}} > r_{\mathrm{SM2}} > 1$, with a peak occurring during the first decades (Fig. 7). We find

https://doi.org/10.5194/tc-2021-327
Preprint. Discussion started: 19 October 2021


The Cryosphere Discussions

that higher local melt rates (small $w$ and/or $P$) favor higher cFRN ratios. They stabilize at values of up to 2.5 towards the end of the perturbation period. However, within the first few model years the majority of the experiments shows larger cFRN values in the ice-stream case than in the shear-margin case, i.e., $r_{\mathrm{SM1}}, r_{\mathrm{SM2}} < 1$ (insets in Fig. 7). This ratio reverts in most cases after about five to ten model years, with high local melt rates favoring a faster transition. Within this short initial period the flux of the ice stream increases to a level that limits the melt-induced central ice-shelf thinning to such an extent that the response to this thinning is outweighed by the response to the less-attenuated shear-margin thinning.

We conduct all three perturbation experiments for different widths $w$ of the basal-melt strip(s) and different perturbation strengths (total melt rates $P$). Overall, the magnitude of the simulated ice-sheet response increases with decreasing $w$ (Figs. 8, A3, A4, A5). A reduction of $w$ under a fixed $P$ value increases the local melt rates (each halving of $w$ doubles the local melt rate) and thus causes higher ice-shelf thinning rates close to the grounding line. This leads to a larger buttressing reduction, explaining the larger increase in grounded ice loss and grounding-line retreat. However, in case of a low perturbation strength and a small melt-strip width the above relation does not apply for the IS experiments where differences in the cFRN between $w = 2$ and $4\ \mathrm{km}$ are small or even reversed. The general increase in the cFRN with declining $w$ is much stronger in the SM1/SM2 experiments than in the IS experiments. This is due to the fact that a reduction in $w$ concentrates the basal melting closer to the grounding line, i.e., in the SM1/SM2 experiments the melting is shifted towards the stagnant lateral ice-shelf margins where the upstream ice supply is sparse, leading to enhanced local thinning rates and, in turn, a stronger ice-sheet response. For the three largest applied shear-margin melt rates (simulations SM1 with $w = 2\ \mathrm{km}$ for $P = 1.5\ \mathrm{Gt/yr}$ and $w = 2/4\ \mathrm{km}$ for $P = 2\ \mathrm{Gt/yr}$) the thinning is intense enough to locally reduce the ice-shelf thickness to zero (cut-off curves in Fig. 7). Due to the lack of comparability these experiments are excluded from the analysis (no data points in Figs. 8 and A2-A5).

The spread in the cFRN under a variation in $P$ for a given $w$ is much larger in the IS experiments (standard deviations in the cFRN, $\sigma_{\mathrm{cFRN}}$, range from around 0.4 and 0.6) than in the SM1/SM2 experiments ($\sigma_{\mathrm{cFRN}}$ between 0.07 to 0.12). A large spread indicates a non-linear response of the grounded ice to different perturbation strengths. In the ice-stream case the lowest perturbation strength ($P = 0.5\ \mathrm{Gt/yr}$) is by far the most efficient one, yielding the largest cFRN value regardless of the melt-strip width. The same applies to the shear-margin melt patterns but only for the medium/wide melt-strip widths $w = 8$ and $16\ \mathrm{km}$, while for smaller $w$ there is no optimal $P$ and the cFRN values lie close to one another.

## 4 Discussion and conclusions

Carrying out idealized numerical simulations we investigate the transient response of a three-dimensional, inherently buttressed marine ice-sheet-shelf system (Figs. 1, 2 and A1) to basal melt perturbations that are applied close to the grounding line in the central ice-stream (IS) region and the lateral shear-margin (SM1/SM2) regions of the ice shelf (Fig. 3). The applied perturbations thin the ice shelf (Fig. 5) and thus reduce its buttressing strength (Figs. A2, A3), inducing an increase in ice discharge across the grounding line (Figs. 4, 8, A4). Our analysis reveals that the flux response strongly depends on the duration, the location, the extent and the strength of the perturbation:

https://doi.org/10.5194/tc-2021-327
Preprint. Discussion started: 19 October 2021


1) The initial change in grounding-line flux (within a few years) is slightly larger for the case of ice-stream melting compared to shear-margin melting (insets of Fig. 7). This is in line with results from Reese et al. (2018) who find strongest instantaneous responses in the grounding-line flux for thinning directly downstream of the grounded Antarctic outlets (comparable to the central ice-stream melt region here). Diagnostic experiments based on the same topographic setup as used in our study show a similar instantaneous response to melting in the ice stream and along the shear margins, respectively (Fig. 2 of Zhang et al. (2020)).

2) For continued melting (more than the initial five to ten years) the flux response becomes significantly stronger to shear-margin melt, being up to 2.5 times as large in the SM1/SM2 case compared to the IS case after 100 model years (Fig. 7). Accompanying induced changes in the upstream grounded ice, i.e., flow acceleration and thinning, as well as grounding-line retreat are much more pronounced under shear-margin melting (Figs. 5, 6, A5). The reason for the differing response magnitudes lies in the topographic characteristics of the simulated ice-sheet-shelf system, that serves as an idealized and simplified representation of a fast-flowing, laterally strongly confined Antarctic-type outlet glacier. Due to the nature of such a channelized ice stream, the major portion of the ice discharge across the grounding line occurs in the central part of the bed trough, i.e., the fast-flowing ice stream (Figs. 2 and A1), and also the induced increase in discharge is strongest there. In the IS melt case the response limits the effect of the perturbation to some extent as the ample supply of ice, which is advected through the ice-stream center, dampens the central ice-shelf thinning. This mechanism is weaker in the SM1/SM2 melt experiments in which the melting takes places under the ice shelf's shear margins where the ice supply is much weaker than in the center. This way, the dampening of the shear-margin thinning is comparably weak, thus resulting in a stronger buttressing reduction and, in turn, a stronger ice-sheet response. Reese et al. (2018) argue that the flux response is an increasing function of thinning, consistent with the above-described increase of the signal from shear-margin melting over the one from ice-stream melting with time.

3) A stronger response is generally favored by a strong perturbation (large $P$) and a high concentration of melting close to the grounding line (small $w$; Fig. 8). Comparing confined to distributed melting in our simulations for a given perturbation strength reveals less grounding-line retreat (Fig. A5) and a smaller increase in ice discharge across the grounding line (Fig. A4) in the case of more distributed melting. This is in agreement with results from idealized flowline simulations of a buttressed ice-sheet-shelf system by Gagliardini et al. (2010). They find grounding-line advance accompanied by volume gain when reducing the concentration of sub-ice-shelf melting to the grounding line, while leaving constant the total amount of melted ice.

There are several simplifications in the design of the model setup and the experiments (shallow stress balance, isothermal ice, idealized bed topography and perturbation, fixed calving front), thus reducing complexity of modeled ice flow. At the same time our approach allows for an analysis that is focused on the essential effects of a perturbation to the ice-shelf bottom on the ice dynamics, isolated from unwanted (secondary) effects that would result from a more complex model realization, while our simulations still incorporate the relevant physics of ice flow. The synthetic bed topography and the idealized forcing used here aim at a conceptual understanding of the ice-sheet response to the applied perturbation in contrast to the attempt of investigating a real-world system that would include a much wider range of physical effects. For instance, the smooth bed geometry used here does not account for bumps usually found in observations of the sub-glacial topography and which would interfere with

https://doi.org/10.5194/tc-2021-327
Preprint. Discussion started: 19 October 2021


grounding-line dynamics (e.g., Alley et al., 2007; Favier et al., 2012). Also, the distribution of the sub-shelf melting in space and their evolution in time would be much more complex in a real-world system (e.g., Dutrieux et al., 2013) in contrast to the spatially very confined, step-like perturbations applied in our simulations. However, the approach taken here allows for an analysis of the first-order effects on ice-shelf buttressing, ice discharge and grounding-line migration. The simplicity of the applied perturbations facilitates the differentiation of the mechanisms underlying the ice-sheet response to ice-shelf thinning in the ice-stream and shear-margin grounding-line regions, respectively.

To put the magnitudes of the applied perturbations into context we can assume that in the simplest case (1) sub-ice-shelf melt rates are approximately linearly correlated to ocean temperatures, increasing by $10\,\mathrm{m\,yr^{-1}}$ for each Kelvin, as estimated by Rignot and Jacobs (2002), and (2) ocean temperatures increase by about $0.1$ to $0.3\,\mathrm{K}$ per decade (supported by evidence in Schmidtko et al., 2014). Extrapolating this trend into the near future yields a possible increase of meltrates of several $10\,\mathrm{m\,yr^{-1}}$ within this century, which is consistent with the local meltrate perturbations applied here (ranging from the orders of $\sim 1\,\mathrm{m\,yr^{-1}}$ to $\sim 10\,\mathrm{m\,yr^{-1}}$).

Our simulations do not account for the process of ice-shelf fracturing (Schulson and Duval, 2009). In fact, basal melting in ice-shelf shear margins that are prone to fracture-induced mechanical weakening can amplify the fracturing and thus diminish the ice shelf's backforce in addition to the purely thinning-induced buttressing reduction (Shepherd, 2003; Borstad et al., 2016; Goldberg et al., 2019). Thus our results likely underestimate the ice-sheet response to melting in the ice-shelf shear margins. Further variables whose analysis is beyond the scope of our study include the length and the width of the ice-shelf embayment as well as the ice rheology. All of these parameters substantially influence the buttressing strength of the ice shelf (Dupont and Alley, 2005; Goldberg et al., 2009; Gudmundsson et al., 2012) and thus their variation might alter our results.

Our findings underline the important role of ice dynamics in the regions adjacent to the grounding line (grounded and floating regimes) interacting with enhanced sub-ice-shelf melting to regulate grounded mass loss. In particular, our results suggest that the dynamics of fast, marine, outlet glaciers that are buttressed by a laterally confined ice shelf - a configuration that is often found in Antarctica - are particularly susceptible to melting in the stagnant, but buttressing-relevant parts of their ice shelves. These regions could include lateral ice-stream margins (as in our simulations) or the vicinity of ice rises. Observational evidence for the occurrence of elevated sub-ice-shelf melting in such regions exists at least occasionally around the Antarctic Ice Sheet, e.g., for Pine Island Ice Shelf (Shean et al., 2019) and Crosson/Dotson ice shelves (Goldberg et al., 2019) in the Amundsen Sea in West Antarctica, Roi Baudouin Ice Shelf, East Antarctica (Berger et al., 2017) or Filchner-Ronne Ice Shelf (Adusumilli et al., 2020). According to our results, melting in such regions does not have to be widespread but can be relatively localized to induce a larger sea-level contribution of the grounded ice sheet compared to melting in the faster moving, central streaming parts of an ice shelf, where the strongest present-day melt rates are usually observed. The underlying mechanism and its implications for global sea-level rise might gain importance in the future as sub-ice-shelf melt rates are expected to increase under continuing global warming.

https://doi.org/10.5194/tc-2021-327
Preprint. Discussion started: 19 October 2021


The Cryosphere Discussions
Open Access
EGU

*Code and data availability.* The code of PISM is openly available at https://pism-docs.org. The simulation data will be made available upon publication.

https://doi.org/10.5194/tc-2021-327
Preprint. Discussion started: 19 October 2021


The Cryosphere Discussions
Open Access
EGU

**Table 1.** Parameters and their values varied throughout the experiments.

| Parameter | Value | Unit | Physical meaning |
|---|---|---|---|
| $a$ | $0.3$ | $\mathrm{m\,yr^{-1}}$ | Surface accumulation rate |
| $A$ | $8 \cdot 10^{-25}$ | $\mathrm{Pa^{-3}\,s^{-1}}$ | Ice softness (Glen's flow law coefficient) |
| $\beta^2$ | $3.16 \cdot 10^{6}$ | $\mathrm{Pa\,m^{-1/3}\,s^{1/3}}$ | Basal friction coefficient in Weertman law (Asay-Davis et al., 2016, Eq. 6) |
| $m$ | $3$ | | Basal friction exponent in Weertman law (Asay-Davis et al., 2016, Eq. 6) |
| $l$ | $21$ | $\mathrm{km}$ | Length of perturbation area |
| $P$ | $\{0.5, 1.0, 1.5, 2.0\}$ | $\mathrm{Gt\,yr^{-1}}$ | Total melt rate in perturbation area |
| $w$ | $\{2, 4, 8, 16\}$ | $\mathrm{km}$ | Width of perturbation area |
| $x_{\mathrm{cf}}$ | $640$ | $\mathrm{km}$ | Position of fixed calving front in right-hand half of domain |

https://doi.org/10.5194/tc-2021-327
Preprint. Discussion started: 19 October 2021


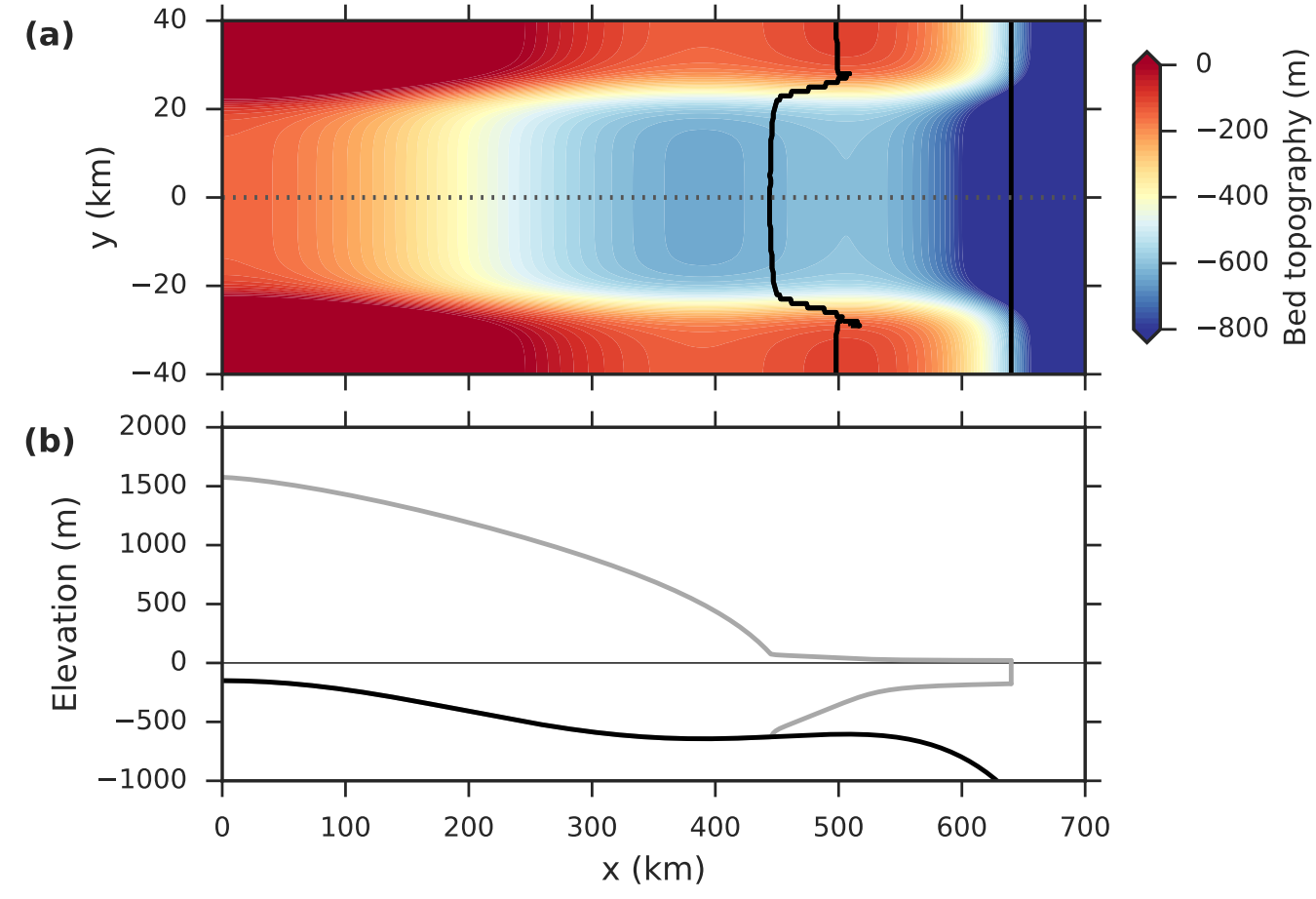


**Figure 1. (a)** Top view of channel-type bed topography (Asay-Davis et al., 2016; Cornford et al., 2020) used in this study, characterized by an overdeepening (retrograde bed section) in $x$-direction on which the spun-up grounding line (black contour) stabilizes. **(b)** Centerline profiles (along dotted line of panel **(a)**) of the spun-up ice-sheet-shelf system (grey) and the underlying bed topography (black).

https://doi.org/10.5194/tc-2021-327
Preprint. Discussion started: 19 October 2021


The Cryosphere Discussions
Open Access
EGU

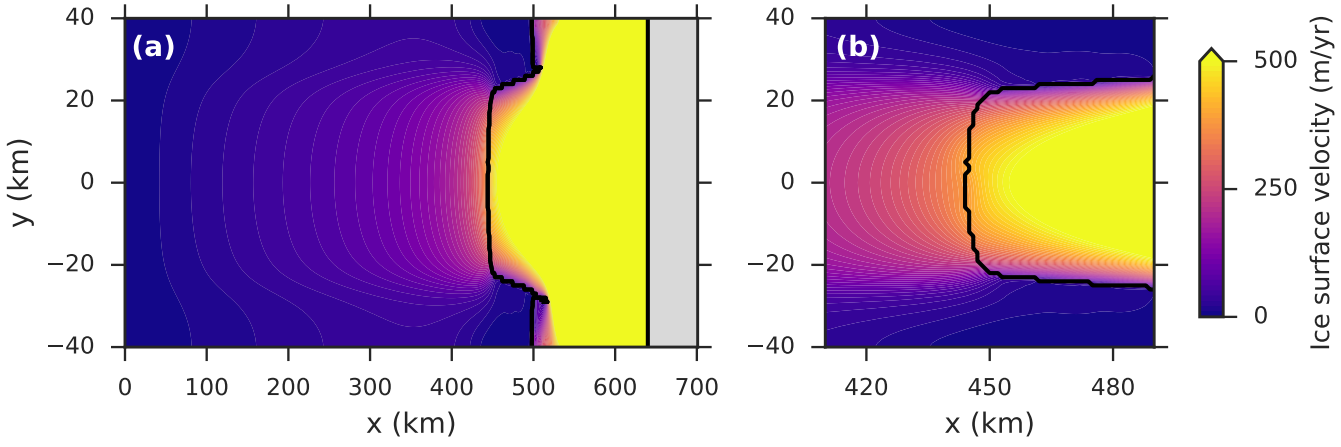


**Figure 2.** Steady-state ice surface speed (colorbar) for **(a)** the entire model domain and **(b)** the grounding-line region. Grounding line and calving front represented by black contours.

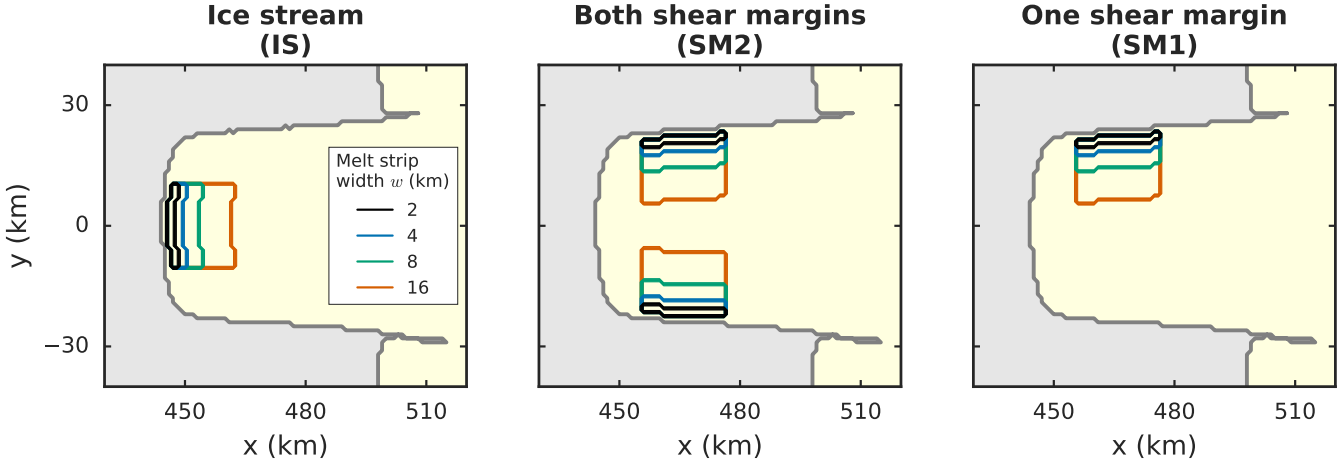


**Figure 3.** Region and spatial extent (colored contours) of the basal-melt perturbations applied in the three types of experiments (zoom into grounding-line region). The steady-state grounding line is represented by the dark grey contour, the ice sheet is colored light gray, the floating ice shelf is colored yellow.

https://doi.org/10.5194/tc-2021-327
Preprint. Discussion started: 19 October 2021


The Cryosphere Discussions
Open Access
EGU

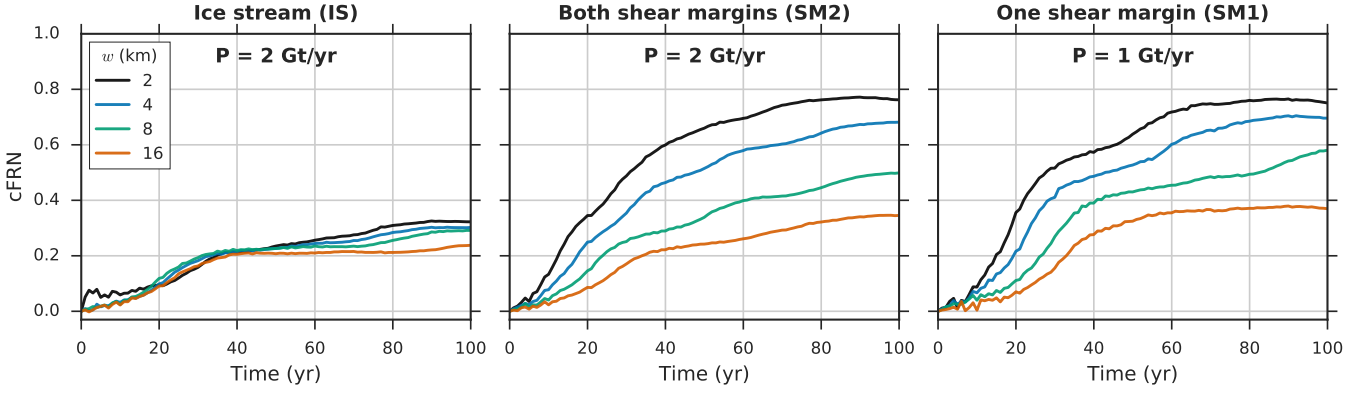


**Figure 4.** Time evolution of the cumulative flux response number, cFRN (Eq. 1), for the three different perturbation experiments.

https://doi.org/10.5194/tc-2021-327
Preprint. Discussion started: 19 October 2021


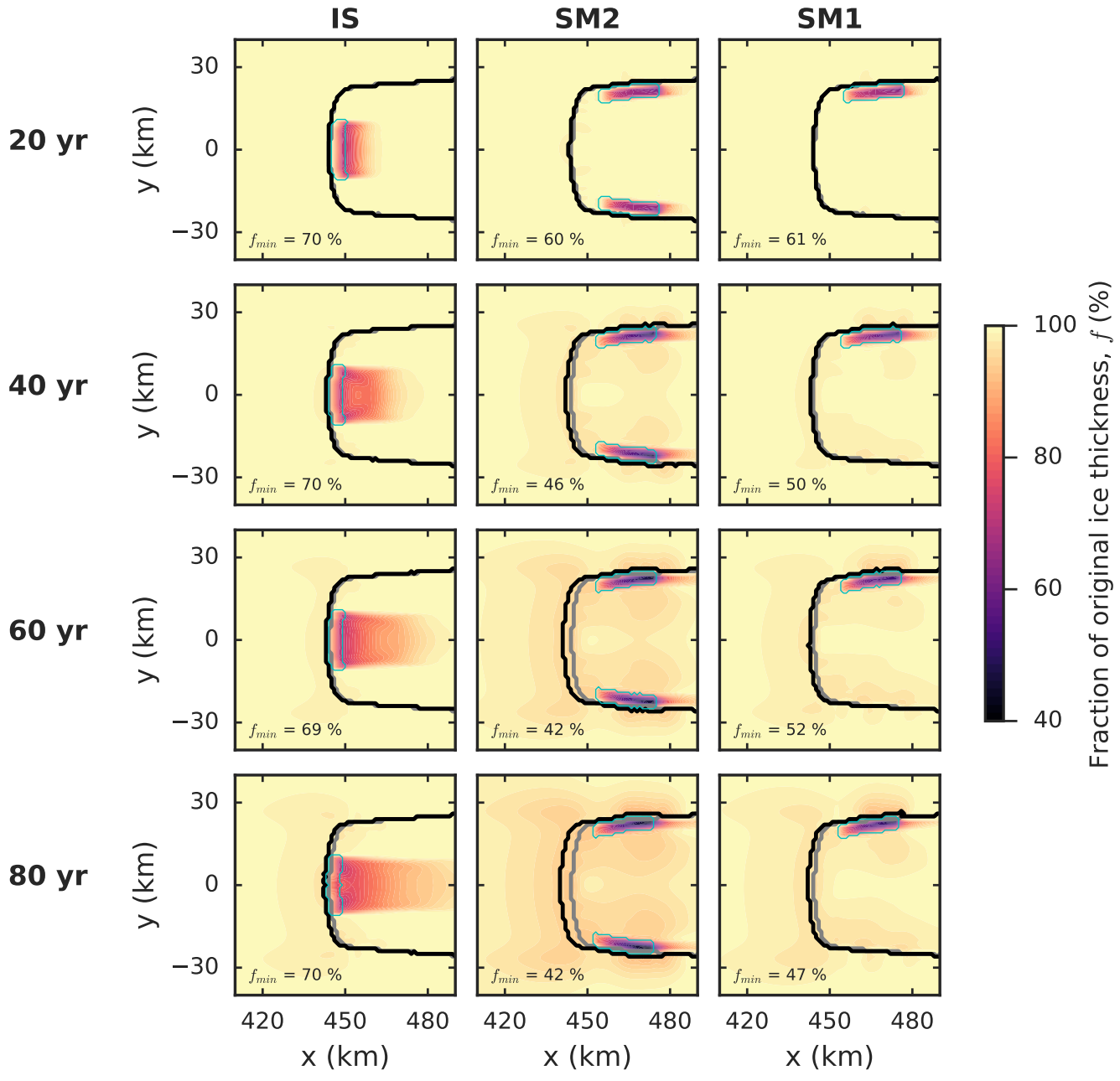


**Figure 5.** Fraction of initial ice thickness $f$ (colorbar) in the vicinity of the grounding line for the three different perturbation types (columns) at time slices of $20, 40, 60$ and $80$ yr after the perturbation onset (rows). In each panel the minimum value of $f$ is given in the lower left corner. Thick contours represent the grounding-line position in the initial state (grey) and in the perturbed states (black). The thin cyan contour denotes the perturbation area. Note that the total melt rate $P$ is 2 $\mathrm{Gt/yr}$ in the IS and SM2 cases and 1 $\mathrm{Gt/yr}$ in the SM1 case for a better comparability between the SM1 and SM2 cases.

https://doi.org/10.5194/tc-2021-327
Preprint. Discussion started: 19 October 2021


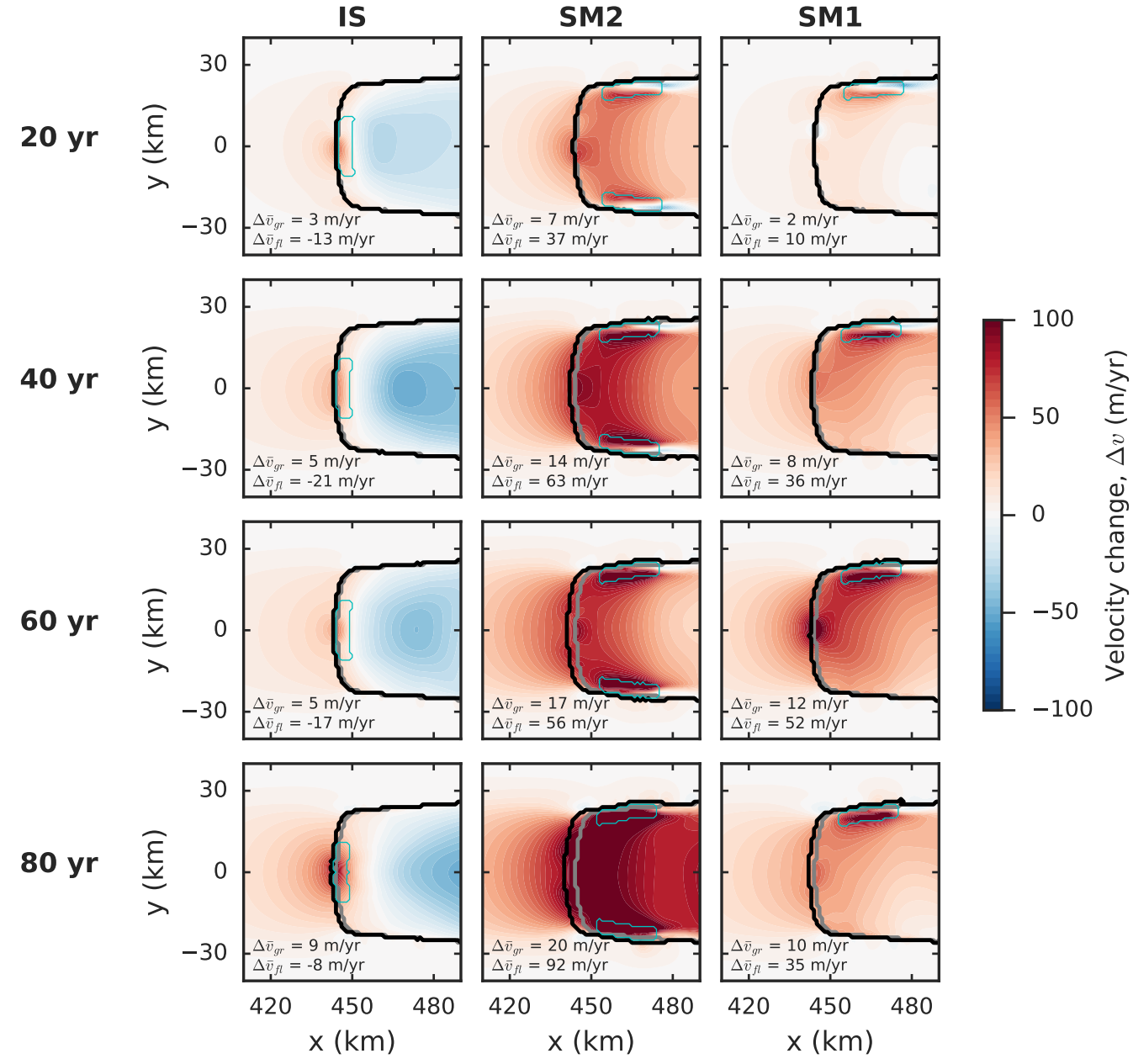


**Figure 6.** Change in ice speed $\Delta v$ (colorbar) in the vicinity of the grounding line for the three different perturbation types (columns) at time slices of $20, 40, 60$ and $80$ yr after the perturbation onset (rows). In each panel the spatial mean of the grounded and floating speed changes (average over the displayed area), $\Delta\bar{v}_{gr}$ and $\Delta\bar{v}_{fl}$, respectively, are given in the lower left corner. Thick contours represent the grounding-line position in the initial state (grey) and in the perturbed states (black). The thin cyan contour denotes the perturbation area. Note that the total melt rate $P$ is $2$ Gt/yr in the IS and SM2 cases and $1$ Gt/yr in the SM1 case for a better comparability between the SM1 and SM2 cases.

https://doi.org/10.5194/tc-2021-327
Preprint. Discussion started: 19 October 2021


The Cryosphere Discussions
Open Access
EGU

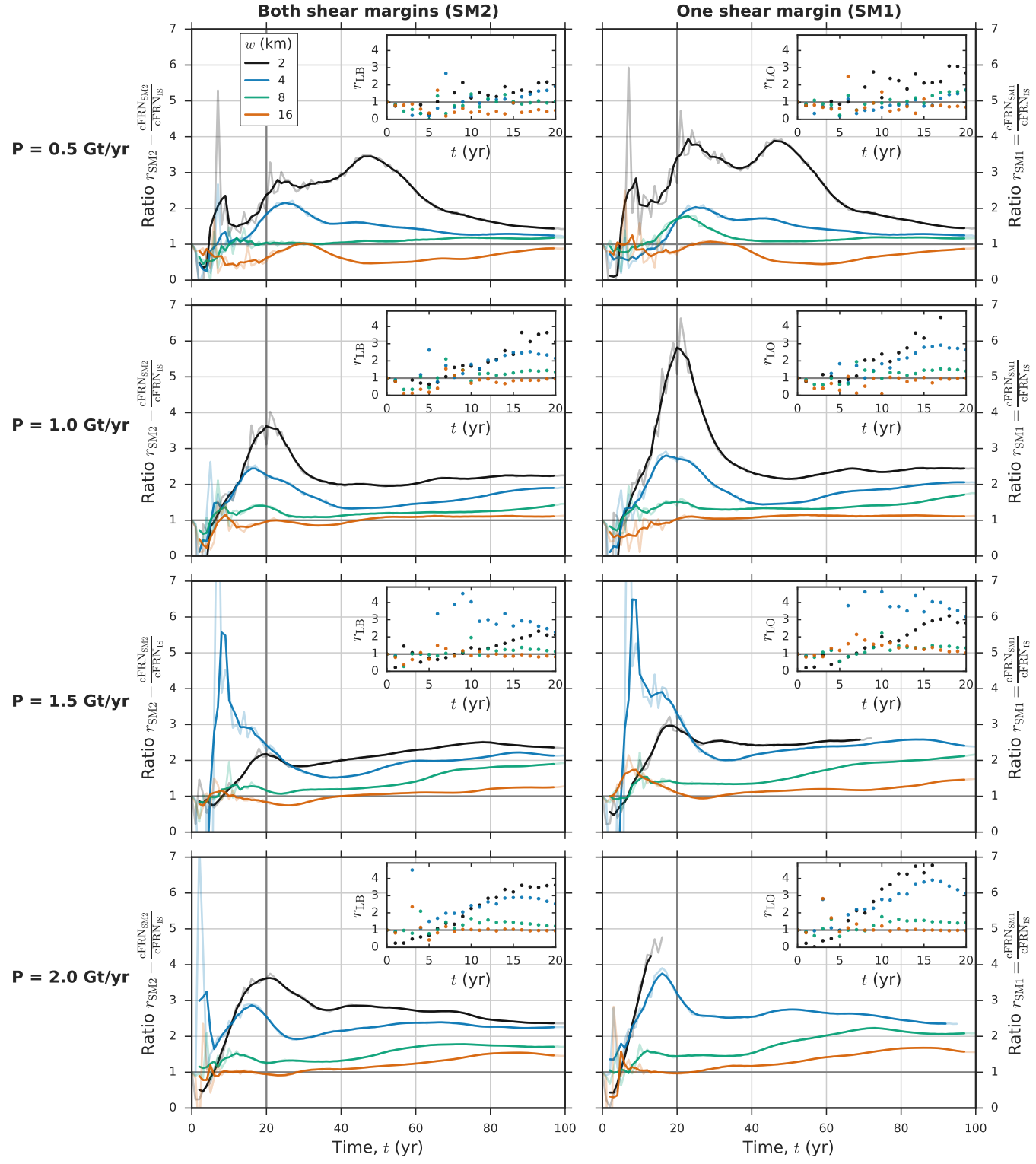


**Figure 7.** Time evolution of the cFRN ratios $r_{SM2}$ and $r_{SM1}$ for the two shear-margin perturbation experiments (columns), respectively, the four perturbation strengths $P$ (rows) and the four melt strip widths $w$ (colors given in the legend). The curves show the 5-year running mean of the yearly data (light colors). For each panel the yearly data points for the first 20 model years are shown in the corresponding inset.

https://doi.org/10.5194/tc-2021-327
Preprint. Discussion started: 19 October 2021


The Cryosphere
Discussions
Open Access
EGU

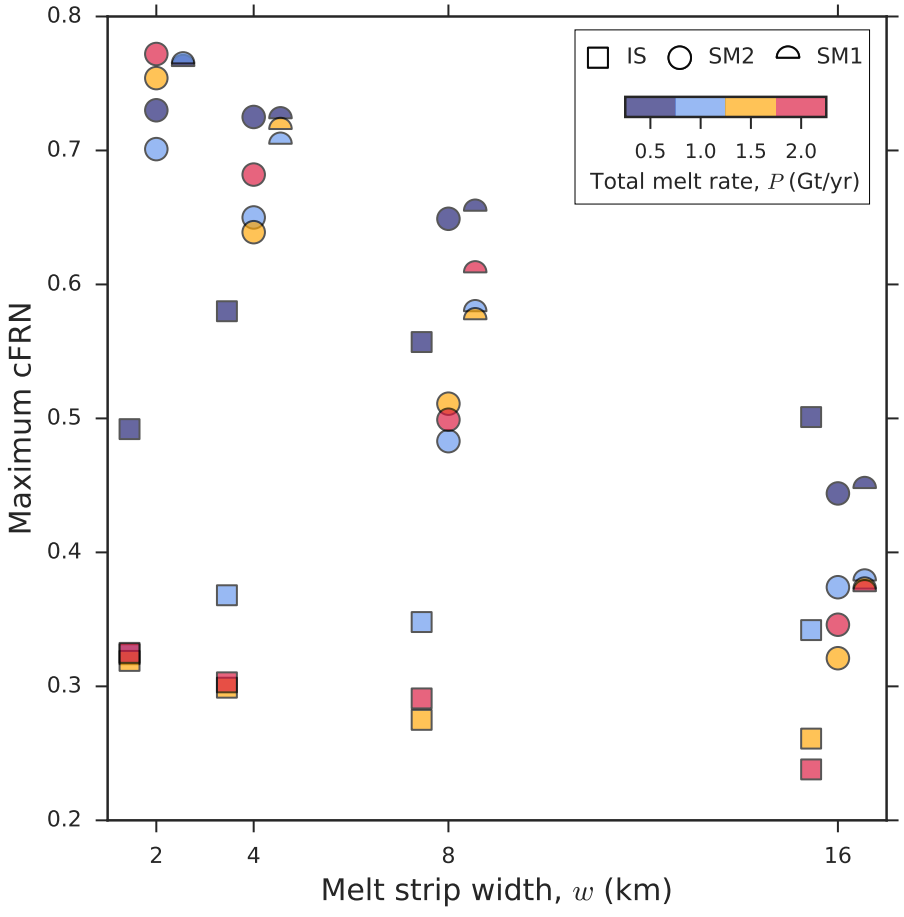


**Figure 8.** Maximum of the cFRN dependent on the melt-strip width $w$ ($x$-axis) and perturbation strength $P$ (colorbar). The perturbation types are represented by individual symbols (legend). For better visibility the data points of the three perturbation types are slightly shifted against each other on the $x$-axis.

https://doi.org/10.5194/tc-2021-327
Preprint. Discussion started: 19 October 2021


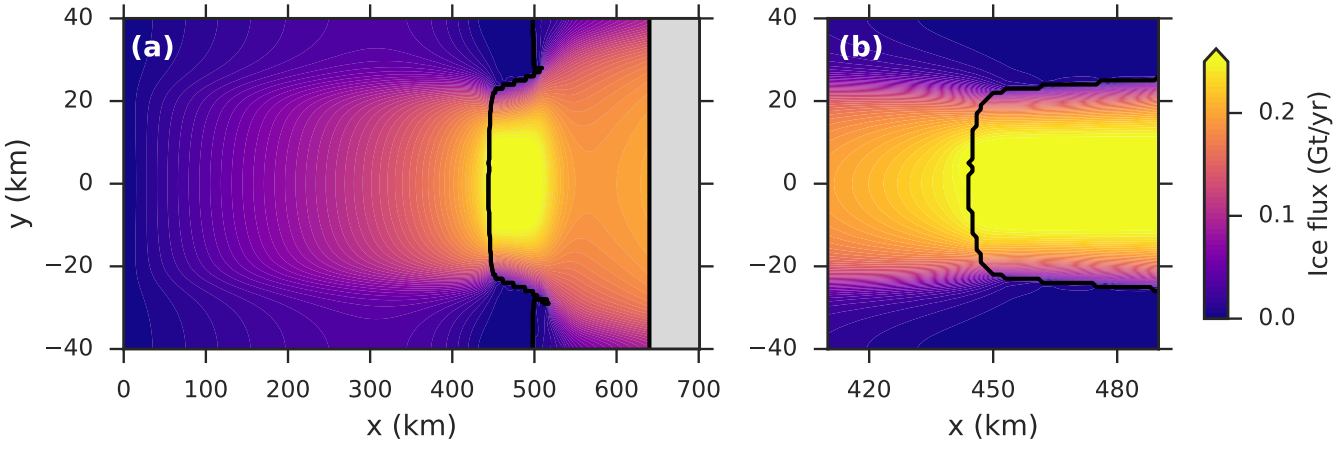


**Figure A1.** Steady-state ice flux magnitude (colorbar) for **(a)** the entire model domain and **(b)** the grounding-line region. Grounding line and calving front represented by black contours.

https://doi.org/10.5194/tc-2021-327
Preprint. Discussion started: 19 October 2021


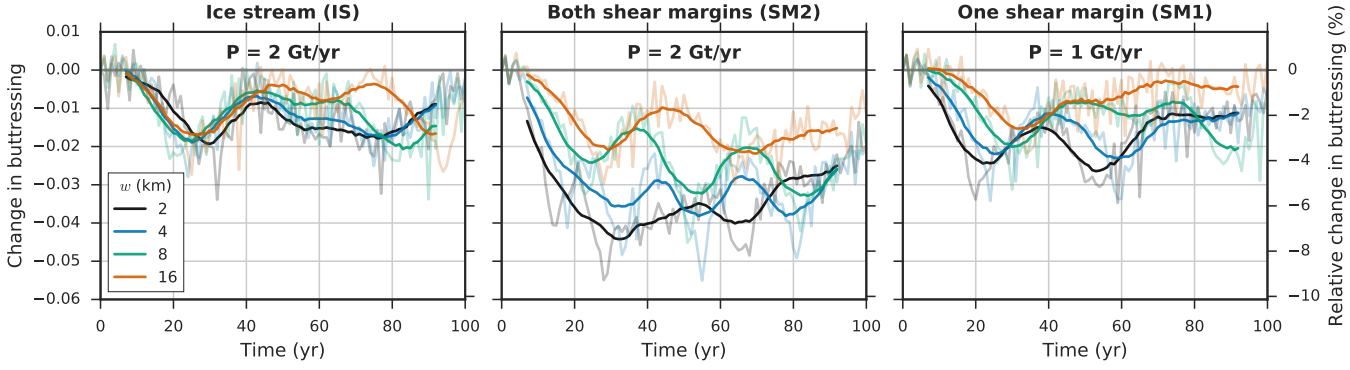


**Figure A2.** Time evolution of the buttressing number in response to the three perturbation types (columns) under a variation of the melt strip width (legend). The grounding-line retreat moderates the buttressing loss as the ice-shelf length increases (Dupont and Alley, 2005; Goldberg et al., 2009) and the perturbation area, tracking the grounding line, is shifted into a region of thicker ice. The buttressing number is diagnosed in flow direction (Fürst et al., 2016) in the center of the ice stream. In this specific case it is equivalent to the buttressing number from Gudmundsson et al. (2012) which is diagnosed in normal direction to the grounding line. The curves (legend) show the 15-year running mean of the yearly data (light colors). To reduce fluctuations the buttressing number is averaged over an area that spans the main part of the ice stream in $y$-direction (between $y = \pm 20$ km) and spans the sector between 10 and 20 km upstream of the grounding line in $x$-direction. Note that the total melt rate $P$ is 2 $\mathrm{Gt/yr}$ in the IS and SM2 cases and 1 $\mathrm{Gt/yr}$ in the SM1 case for a better comparability between the SM1 and SM2 cases.

https://doi.org/10.5194/tc-2021-327
Preprint. Discussion started: 19 October 2021


The Cryosphere
Discussions
Open Access
EGU

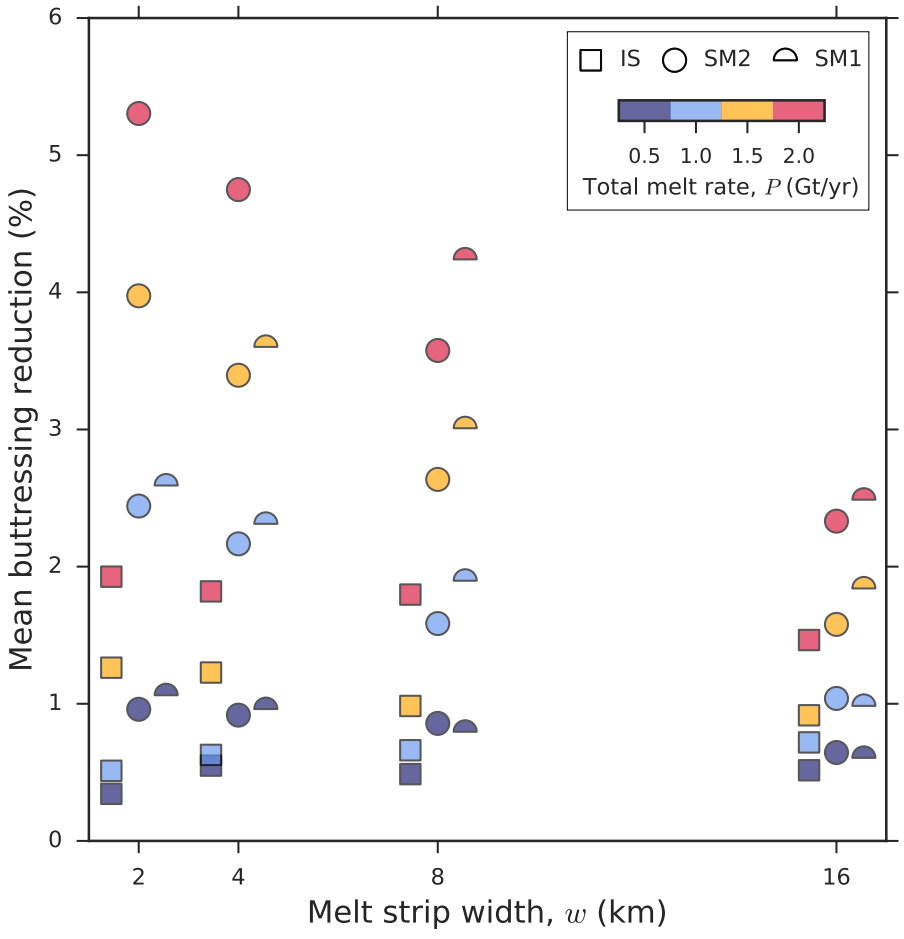


**Figure A3.** Time-averaged buttressing reduction dependent on the melt-strip width $w$ ($x$-axis) and perturbation strength $P$ (colorbar). The perturbation types are represented by individual symbols (legend). For better visibility the data points of the three perturbation types are slightly shifted against each other on the $x$-axis.

https://doi.org/10.5194/tc-2021-327
Preprint. Discussion started: 19 October 2021


The Cryosphere
Discussions
Open Access
EGU

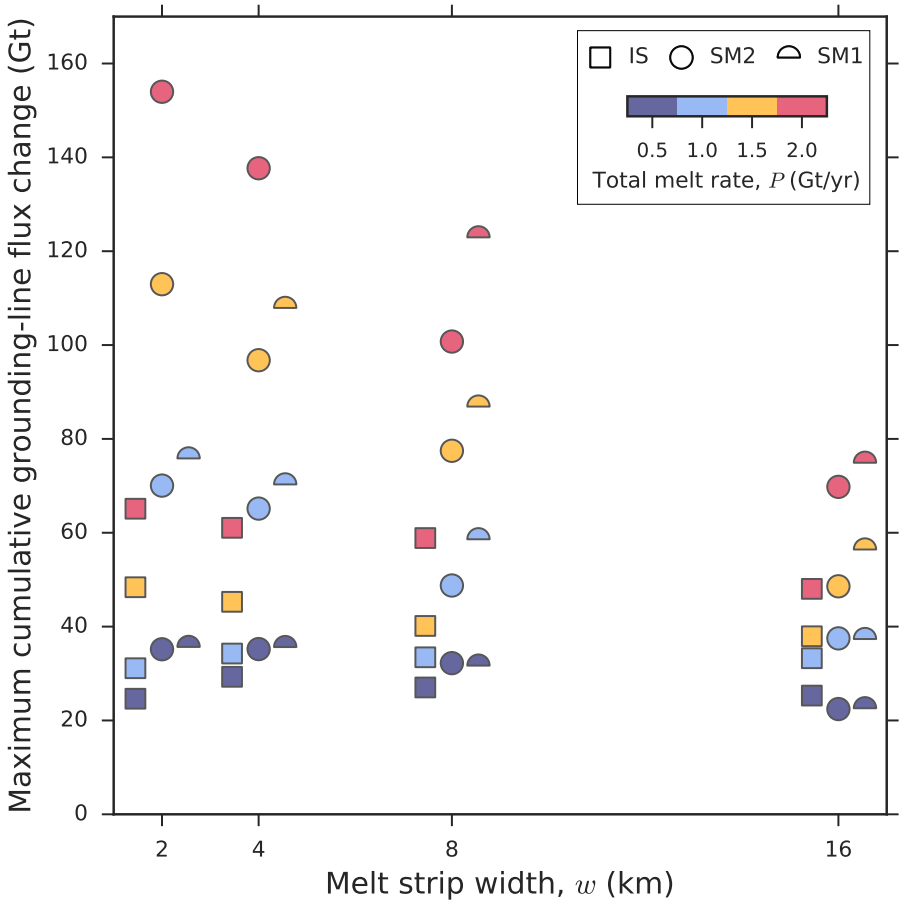


**Figure A4.** Maximum of the cumulative grounding-line-flux change dependent on the melt-strip width $w$ ($x$-axis) and perturbation strength $P$ (colorbar). The perturbation types are represented by individual symbols (legend). For better visibility the data points of the three perturbation types are slightly shifted against each other on the $x$-axis.

https://doi.org/10.5194/tc-2021-327
Preprint. Discussion started: 19 October 2021




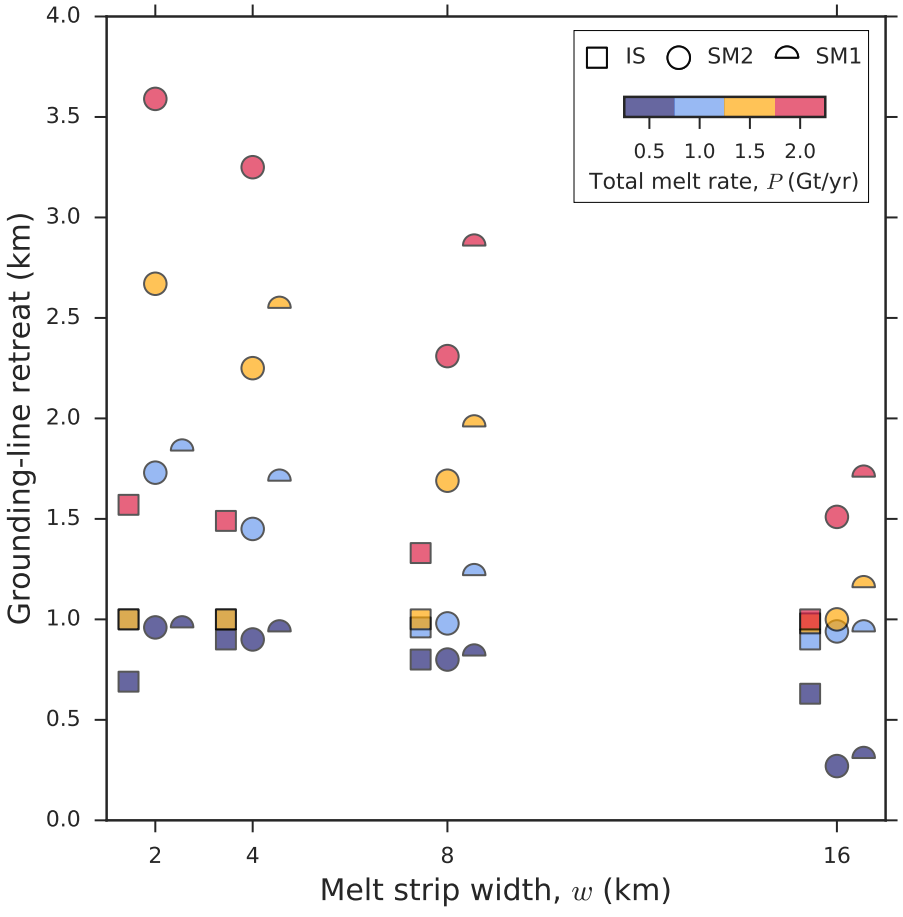


**Figure A5.** Centerline grounding-line retreat (average over the last 50 model years) dependent on the melt-strip width $w$ ($x$-axis) and perturbation strength $P$ (colorbar). The perturbation types are represented by individual symbols (legend). For better visibility the data points of the three perturbation types are slightly shifted against each other on the $x$-axis.

https://doi.org/10.5194/tc-2021-327
Preprint. Discussion started: 19 October 2021




*Competing interests.* The authors declare no conflict of interest.

*Acknowledgements.*

https://doi.org/10.5194/tc-2021-327
Preprint. Discussion started: 19 October 2021




## References

Adusumilli, S., Fricker, H. A., Medley, B., Padman, L., and Siegfried, M. R.: Interannual variations in meltwater input to the Southern Ocean from Antarctic ice shelves, Nature Geoscience, 13, 616–620, https://doi.org/10.1038/s41561-020-0616-z, https://www.nature.com/articles/s41561-020-0616-z, bandiera_abtest: a Cg_type: Nature Research Journals Number: 9 Primary_atype: Research Publisher: Nature Publishing Group Subject_term: Cryospheric science;Physical oceanography Subject_term_id: cryospheric-science;physical-oceanography, 2020.

Alley, R. B., Anandakrishnan, S., Dupont, T. K., Parizek, B. R., and Pollard, D.: Effect of Sedimentation on Ice-Sheet Grounding-Line Stability, Science, 315, 1838–1841, https://doi.org/10.1126/science.1138396, http://www.sciencemag.org/cgi/doi/10.1126/science.1138396, 2007.

Asay-Davis, X. S., Cornford, S. L., Durand, G., Galton-Fenzi, B. K., Gladstone, R. M., Gudmundsson, G. H., Hattermann, T., Holland, D. M., Holland, D., Holland, P. R., Martin, D. F., Mathiot, P., Pattyn, F., and Seroussi, H.: Experimental design for three interrelated marine ice sheet and ocean model intercomparison projects: MISMIP v. 3 (MISMIP +), ISOMIP v. 2 (ISOMIP +) and MISOMIP v. 1 (MISOMIP1), Geoscientific Model Development, 9, 2471–2497, https://doi.org/10.5194/gmd-9-2471-2016, https://www.geosci-model-dev.net/9/2471/2016/, 2016.

Bakker, A. M. R., Wong, T. E., Ruckert, K. L., and Keller, K.: Sea-level projections representing the deeply uncertain contribution of the West Antarctic ice sheet, Scientific Reports, 7, 1–7, https://doi.org/10.1038/s41598-017-04134-5, https://www.nature.com/articles/s41598-017-04134-5, 2017.

Bamber, J. L. and Aspinall, W. P.: An expert judgement assessment of future sea level rise from the ice sheets, Nature Climate Change, 3, 424–427, https://doi.org/10.1038/nclimate1778, http://www.nature.com/articles/nclimate1778, 2013.

Berger, S., Drews, R., Helm, V., Sun, S., and Pattyn, F.: Detecting high spatial variability of ice shelf basal mass balance, Roi Baudouin Ice Shelf, Antarctica, The Cryosphere, 11, 2675–2690, https://doi.org/10.5194/tc-11-2675-2017, https://www.the-cryosphere.net/11/2675/2017/, 2017.

Bindschadler, R. A., Nowicki, S., Abe-Ouchi, A., Aschwanden, A., Choi, H., Fastook, J., Granzow, G., Greve, R., Gutowski, G., Herzfeld, U., Jackson, C., Johnson, J., Khroulev, C., Levermann, A., Lipscomb, W. H., Martin, M. A., Morlighem, M., Parizek, B. R., Pollard, D., Price, S. F., Ren, D., Saito, F., Sato, T., Seddik, H., Seroussi, H., Takahashi, K., Walker, R., and Wang, W. L.: Ice-sheet model sensitivities to environmental forcing and their use in projecting future sea level (the SeaRISE project), Journal of Glaciology, 59, 195–224, https://doi.org/10.3189/2013JoG12J125, https://www.cambridge.org/core/product/identifier/S0022143000204267/type/journal_article, 2013.

Borstad, C., Khazendar, A., Scheuchl, B., Morlighem, M., Larour, E., and Rignot, E.: A constitutive framework for predicting weakening and reduced buttressing of ice shelves based on observations of the progressive deterioration of the remnant Larsen B Ice Shelf, Geophysical Research Letters, 43, 2027–2035, https://doi.org/10.1002/2015GL067365, https://agupubs.onlinelibrary.wiley.com/doi/abs/10.1002/2015GL067365, _eprint: https://agupubs.onlinelibrary.wiley.com/doi/pdf/10.1002/2015GL067365, 2016.

Bueler, E. and Brown, J.: Shallow shelf approximation as a "sliding law" in a thermomechanically coupled ice sheet model, Journal of Geophysical Research, 114, https://doi.org/10.1029/2008JF001179, http://doi.wiley.com/10.1029/2008JF001179, 2009.

Cornford, S. L., Seroussi, H., Asay-Davis, X. S., Gudmundsson, G. H., Arthern, R., Borstad, C., Christmann, J., Dias dos Santos, T., Feldmann, J., Goldberg, D., Hoffman, M. J., Humbert, A., Kleiner, T., Leguy, G., Lipscomb, W. H., Merino, N., Durand, G., Morlighem, M., Pollard, D., Rückamp, M., Williams, C. R., and Yu, H.: Results of the third Marine Ice Sheet Model Intercomparison Project (MISMIP+),


The Cryosphere, 14, 2283–2301, https://doi.org/https://doi.org/10.5194/tc-14-2283-2020, https://tc.copernicus.org/articles/14/2283/2020/, 2020.

Dupont, T. K. and Alley, R. B.: Assessment of the importance of ice-shelf buttressing to ice-sheet flow, Geophysical Research Letters, 32, https://doi.org/10.1029/2004GL022024, https://agupubs.onlinelibrary.wiley.com/doi/abs/10.1029/2004GL022024, 2005.

Dutrieux, P., Vaughan, D. G., Corr, H. F. J., Jenkins, A., Holland, P. R., Joughin, I., and Fleming, A. H.: Pine Island glacier ice shelf melt distributed at kilometre scales, The Cryosphere, 7, 1543–1555, https://doi.org/10.5194/tc-7-1543-2013, https://www.the-cryosphere.net/7/1543/2013/, 2013.

Edwards, T. L., Nowicki, S., Marzeion, B., Hock, R., Goelzer, H., Seroussi, H., Jourdain, N. C., Slater, D. A., Turner, F. E., Smith, C. J., McKenna, C. M., Simon, E., Abe-Ouchi, A., Gregory, J. M., Larour, E., Lipscomb, W. H., Payne, A. J., Shepherd, A., Agosta, C., Alexander, P., Albrecht, T., Anderson, B., Asay-Davis, X., Aschwanden, A., Barthel, A., Bliss, A., Calov, R., Chambers, C., Champollion, N., Choi, Y., Cullather, R., Cuzzone, J., Dumas, C., Felikson, D., Fettweis, X., Fujita, K., Galton-Fenzi, B. K., Gladstone, R., Golledge, N. R., Greve, R., Hattermann, T., Hoffman, M. J., Humbert, A., Huss, M., Huybrechts, P., Immerzeel, W., Kleiner, T., Kraaijenbrink, P., Le Clec'h, S., Lee, V., Leguy, G. R., Little, C. M., Lowry, D. P., Malles, J.-H., Martin, D. F., Maussion, F., Morlighem, M., O'Neill, J. F., Nias, I., Pattyn, F., Pelle, T., Price, S. F., Quiquet, A., Radić, V., Reese, R., Rounce, D. R., Rückamp, M., Sakai, A., Shafer, C., Schlegel, N.-J., Shannon, S., Smith, R. S., Straneo, F., Sun, S., Tarasov, L., Trusel, L. D., Van Breedam, J., van de Wal, R., van den Broeke, M., Winkelmann, R., Zekollari, H., Zhao, C., Zhang, T., and Zwinger, T.: Projected land ice contributions to twenty-first-century sea level rise, Nature, 593, 74–82, https://doi.org/10.1038/s41586-021-03302-y, https://www.nature.com/articles/s41586-021-03302-y, 2021.

Favier, L., Gagliardini, O., Durand, G., and Zwinger, T.: A three-dimensional full Stokes model of the grounding line dynamics: effect of a pinning point beneath the ice shelf, The Cryosphere, 6, 101–112, https://doi.org/10.5194/tc-6-101-2012, https://www.the-cryosphere.net/6/101/2012/, 2012.

Favier, L., Durand, G., Cornford, S. L., Gudmundsson, G. H., Gagliardini, O., Gillet-Chaulet, F., Zwinger, T., Payne, A. J., and Le Brocq, A. M.: Retreat of Pine Island Glacier controlled by marine ice-sheet instability, Nature Climate Change, 4, 117–121, https://doi.org/10.1038/nclimate2094, http://www.nature.com/articles/nclimate2094, 2014.

Feldmann, J., Albrecht, T., Khroulev, C., Pattyn, F., and Levermann, A.: Resolution-dependent performance of grounding line motion in a shallow model compared with a full-Stokes model according to the MISMIP3d intercomparison, Journal of Glaciology, 60, 353–360, https://doi.org/10.3189/2014JoG13J093, https://www.cambridge.org/core/product/identifier/S0022143000205406/type/journal_article, 2014.

Fürst, J. J., Durand, G., Gillet-Chaulet, F., Tavard, L., Rankl, M., Braun, M., and Gagliardini, O.: The safety band of Antarctic ice shelves, Nature Climate Change, 6, 479–482, https://doi.org/10.1038/nclimate2912, http://www.nature.com/articles/nclimate2912, 2016.

Gagliardini, O., Durand, G., Zwinger, T., Hindmarsh, R. C. A., and Le Meur, E.: Coupling of ice-shelf melting and buttressing is a key process in ice-sheets dynamics: ICE-SHELF MELTING AND BUTTRESSING, Geophysical Research Letters, 37, n/a–n/a, https://doi.org/10.1029/2010GL043334, http://doi.wiley.com/10.1029/2010GL043334, 2010.

Goldberg, D., Holland, D. M., and Schoof, C.: Grounding line movement and ice shelf buttressing in marine ice sheets, Journal of Geophysical Research, 114, https://doi.org/10.1029/2008JF001227, http://doi.wiley.com/10.1029/2008JF001227, 2009.

Goldberg, D. N., Gourmelen, N., Kimura, S., Millan, R., and Snow, K.: How Accurately Should We Model Ice Shelf Melt Rates?, Geophysical Research Letters, 46, 189–199, https://doi.org/10.1029/2018GL080383, https://agupubs.onlinelibrary.wiley.com/doi/abs/10.1029/2018GL080383, 2019.


Greve, R. and Blatter, H.: Dynamics of Ice Sheets and Glaciers, Advances in Geophysical and Environmental Mechanics and Mathematics, Springer Berlin Heidelberg, Berlin, Heidelberg, https://doi.org/10.1007/978-3-642-03415-2, http://link.springer.com/10.1007/978-3-642-03415-2, 2009.

Gudmundsson, G. H., Krug, J., Durand, G., Favier, L., and Gagliardini, O.: The stability of grounding lines on retrograde slopes, The Cryosphere, 6, 1497–1505, https://doi.org/10.5194/tc-6-1497-2012, https://www.the-cryosphere.net/6/1497/2012/, 2012.

Haseloff, M. and Sergienko, O. V.: The effect of buttressing on grounding line dynamics, Journal of Glaciology, 64, 417–431, https://doi.org/10.1017/jog.2018.30, https://www.cambridge.org/core/product/identifier/S0022143018000308/type/journal_article, 2018.

Hellmer, H. H., Kauker, F., Timmermann, R., Determann, J., and Rae, J.: Twenty-first-century warming of a large Antarctic ice-shelf cavity by a redirected coastal current, Nature, 485, 225–228, https://doi.org/10.1038/nature11064, http://www.nature.com/doifinder/10.1038/nature11064, 2012.

Hutter, K.: Theoretical Glaciology: Material Science of Ice and the Mechanics of Glaciers and Ice Sheets (Mathematical Approaches to Geophysics), Reidel Publishing Company/Terra Scientific Publishing Company, 1983.

Jackson, L. P., Grinsted, A., and Jevrejeva, S.: 21st Century Sea-Level Rise in Line with the Paris Accord, Earth's Future, 6, 213–229, https://doi.org/10.1002/2017EF000688, http://doi.wiley.com/10.1002/2017EF000688, 2018.

Jenkins, A., Dutrieux, P., Jacobs, S. S., McPhail, S. D., Perrett, J. R., Webb, A. T., and White, D.: Observations beneath Pine Island Glacier in West Antarctica and implications for its retreat, Nature Geoscience, 3, 468–472, https://doi.org/10.1038/ngeo890, http://www.nature.com/articles/ngeo890, 2010.

Joughin, I. and Alley, R. B.: Stability of the West Antarctic ice sheet in a warming world, Nature Geoscience, 4, 506–513, https://doi.org/10.1038/ngeo1194, http://www.nature.com/articles/ngeo1194, 2011.

Joughin, I., Smith, B. E., and Medley, B.: Marine Ice Sheet Collapse Potentially Under Way for the Thwaites Glacier Basin, West Antarctica, Science, 344, 735–738, https://doi.org/10.1126/science.1249055, http://www.sciencemag.org/cgi/doi/10.1126/science.1249055, 2014.

Khroulev, C. and Authors, P.: PISM, a Parallel Ice Sheet Model v1.0. Users's Manual, http://www.pism-docs.org, 2020.

Konrad, H., Shepherd, A., Gilbert, L., Hogg, A. E., McMillan, M., Muir, A., and Slater, T.: Net retreat of Antarctic glacier grounding lines, Nature Geoscience, 11, 258–262, https://doi.org/10.1038/s41561-018-0082-z, http://www.nature.com/articles/s41561-018-0082-z, 2018.

Levermann, A., Winkelmann, R., Albrecht, T., Goelzer, H., Golledge, N. R., Greve, R., Huybrechts, P., Jordan, J., Leguy, G., Martin, D., Morlighem, M., Pattyn, F., Pollard, D., Quiquet, A., Rodehacke, C., Seroussi, H., Sutter, J., Zhang, T., Van Breedam, J., Calov, R., DeConto, R., Dumas, C., Garbe, J., Gudmundsson, G. H., Hoffman, M. J., Humbert, A., Kleiner, T., Lipscomb, W. H., Meinshausen, M., Ng, E., Nowicki, S. M. J., Perego, M., Price, S. F., Saito, F., Schlegel, N.-J., Sun, S., and van de Wal, R. S. W.: Projecting Antarctica's contribution to future sea level rise from basal ice shelf melt using linear response functions of 16 ice sheet models (LARMIP-2), Earth System Dynamics, 11, 35–76, https://doi.org/10.5194/esd-11-35-2020, https://esd.copernicus.org/articles/11/35/2020/, publisher: Copernicus GmbH, 2020.

Mengel, M. and Levermann, A.: Ice plug prevents irreversible discharge from East Antarctica, Nature Climate Change, 4, 451–455, https://doi.org/10.1038/nclimate2226, http://www.nature.com/articles/nclimate2226, 2014.

Morland, L. W.: Unconfined Ice-Shelf Flow, in: Dynamics of the West Antarctic Ice Sheet, edited by Van der Veen, C. J. and Oerlemans, J., Glaciology and Quaternary Geology, pp. 99–116, Springer Netherlands, 1987.

Naughten, K. A., Meissner, K. J., Galton-Fenzi, B. K., England, M. H., Timmermann, R., and Hellmer, H. H.: Future Projections of Antarctic Ice Shelf Melting Based on CMIP5 Scenarios, Journal of Climate, 31, 5243–5261, https://doi.org/10.1175/JCLI-D-17-0854.1, https://journals.ametsoc.org/doi/full/10.1175/JCLI-D-17-0854.1, 2018.

https://doi.org/10.5194/tc-2021-327
Preprint. Discussion started: 19 October 2021




Paolo, F. S., Fricker, H. A., and Padman, L.: Volume loss from Antarctic ice shelves is accelerating, Science, 348, 327–331, https://doi.org/10.1126/science.aaa0940, https://science.sciencemag.org/content/348/6232/327, 2015.

Pattyn, F., Perichon, L., Durand, G., Favier, L., Gagliardini, O., Hindmarsh, R. C., Zwinger, T., Albrecht, T., Cornford, S., Docquier, D., Fürst, J. J., Goldberg, D., Gudmundsson, G. H., Humbert, A., Hütten, M., Huybrechts, P., Jouvet, G., Kleiner, T., Larour, E., Martin, D., Morlighem, M., Payne, A. J., Pollard, D., Rückamp, M., Rybak, O., Seroussi, H., Thoma, M., and Wilkens, N.: Grounding-line migration in plan-view marine ice-sheet models: results of the ice2sea MISMIP3d intercomparison, Journal of Glaciology, 59, 410–422, https://doi.org/10.3189/2013JoG12J129, https://www.cambridge.org/core/product/identifier/S0022143000204425/type/journal_article, 2013.

Payne, A. J., Nowicki, S., Abe-Ouchi, A., Agosta, C., Alexander, P., Albrecht, T., Asay-Davis, X., Aschwanden, A., Barthel, A., Bracegirdle, T. J., Calov, R., Chambers, C., Choi, Y., Cullather, R., Cuzzone, J., Dumas, C., Edwards, T. L., Felikson, D., Fettweis, X., Galton-Fenzi, B. K., Goelzer, H., Gladstone, R., Golledge, N. R., Gregory, J. M., Greve, R., Hattermann, T., Hoffman, M. J., Humbert, A., Huybrechts, P., Jourdain, N. C., Kleiner, T., Munneke, P. K., Larour, E., Le clec'h, S., Lee, V., Leguy, G., Lipscomb, W. H., Little, C. M., Lowry, D. P., Morlighem, M., Nias, I., Pattyn, F., Pelle, T., Price, S. F., Quiquet, A., Reese, R., Rückamp, M., Schlegel, N.-J., Seroussi, H., Shepherd, A., Simon, E., Slater, D., Smith, R. S., Straneo, F., Sun, S., Tarasov, L., Trusel, L. D., Van Breedam, J., van de Wal, R., van den Broeke, M., Winkelmann, R., Zhao, C., Zhang, T., and Zwinger, T.: Future Sea Level Change Under Coupled Model Intercomparison Project Phase 5 and Phase 6 Scenarios From the Greenland and Antarctic Ice Sheets, Geophysical Research Letters, 48, e2020GL091 741, https://doi.org/10.1029/2020GL091741, https://onlinelibrary.wiley.com/doi/abs/10.1029/2020GL091741, _eprint: https://onlinelibrary.wiley.com/doi/pdf/10.1029/2020GL091741, 2021.

Pegler, S. S.: Marine ice sheet dynamics: the impacts of ice-shelf buttressing, Journal of Fluid Mechanics, 857, 605–647, https://doi.org/10.1017/jfm.2018.741, https://www.cambridge.org/core/journals/journal-of-fluid-mechanics/article/abs/marine-ice-sheet-dynamics-the-impacts-of-iceshelf-buttressing/7D5B6566FBA37D08F7AA438DB13FCA76, 2018.

Pollard, D., DeConto, R. M., and Alley, R. B.: Potential Antarctic Ice Sheet retreat driven by hydrofracturing and ice cliff failure, Earth and Planetary Science Letters, 412, 112–121, https://doi.org/10.1016/j.epsl.2014.12.035, https://linkinghub.elsevier.com/retrieve/pii/S0012821X14007961, 2015.

Pritchard, H. D., Ligtenberg, S. R. M., Fricker, H. A., Vaughan, D. G., van den Broeke, M. R., and Padman, L.: Antarctic ice-sheet loss driven by basal melting of ice shelves, Nature, 484, 502–505, https://doi.org/10.1038/nature10968, http://www.nature.com/doifinder/10.1038/nature10968, 2012.

Reese, R., Gudmundsson, G. H., Levermann, A., and Winkelmann, R.: The far reach of ice-shelf thinning in Antarctica, Nature Climate Change, 8, 53–57, https://doi.org/10.1038/s41558-017-0020-x, http://www.nature.com/articles/s41558-017-0020-x, 2018.

Reese, R., Levermann, A., Albrecht, T., Seroussi, H., and Winkelmann, R.: The role of history and strength of the oceanic forcing in sea level projections from Antarctica with the Parallel Ice Sheet Model, The Cryosphere, 14, 3097–3110, https://doi.org/10.5194/tc-14-3097-2020, https://tc.copernicus.org/articles/14/3097/2020/, publisher: Copernicus GmbH, 2020.

Rignot, E. and Jacobs, S.: Rapid Bottom Melting Widespread near Antarctic Ice Sheet Grounding Lines, Science, 296, 2020–2023, https://doi.org/10.1126/science.1070942, http://www.sciencemag.org/cgi/doi/10.1126/science.1070942, 2002.

Rignot, E., Jacobs, S., Mouginot, J., and Scheuchl, B.: Ice-Shelf Melting Around Antarctica, Science, 341, 266–270, https://doi.org/10.1126/science.1235798, http://www.sciencemag.org/cgi/doi/10.1126/science.1235798, 2013.


Rignot, E., Mouginot, J., Morlighem, M., Seroussi, H., and Scheuchl, B.: Widespread, rapid grounding line retreat of Pine Island, Thwaites, Smith, and Kohler glaciers, West Antarctica, from 1992 to 2011, Geophysical Research Letters, 41, 3502–3509, https://doi.org/10.1002/2014GL060140, http://doi.wiley.com/10.1002/2014GL060140, 2014.

Rignot, E., Mouginot, J., Scheuchl, B., Broeke, M. v. d., Wessem, M. J. v., and Morlighem, M.: Four decades of Antarctic Ice Sheet mass balance from 1979–2017, Proceedings of the National Academy of Sciences, 116, 1095–1103, https://doi.org/10.1073/pnas.1812883116, https://www.pnas.org/content/116/4/1095, 2019.

Schmidtko, S., Heywood, K. J., Thompson, A. F., and Aoki, S.: Multidecadal warming of Antarctic waters, Science, 346, 1227–1231, https://doi.org/10.1126/science.1256117, http://science.sciencemag.org/content/346/6214/1227, 2014.

Schoof, C.: Ice sheet grounding line dynamics: Steady states, stability, and hysteresis, Journal of Geophysical Research, 112, https://doi.org/10.1029/2006JF000664, http://doi.wiley.com/10.1029/2006JF000664, 2007.

Schulson, E. M. and Duval, P.: Creep and Fracture of Ice, Cambridge University Press, Cambridge, https://doi.org/10.1017/CBO9780511581397, https://www.cambridge.org/core/books/creep-and-fracture-of-ice/679E87C60A28D40712A28E857F8235CA, 2009.

Shean, D. E., Joughin, I. R., Dutrieux, P., Smith, B. E., and Berthier, E.: Ice shelf basal melt rates from a high-resolution digital elevation model (DEM) record for Pine Island Glacier, Antarctica, The Cryosphere, 13, 2633–2656, https://doi.org/10.5194/tc-13-2633-2019, https://tc.copernicus.org/articles/13/2633/2019/, publisher: Copernicus GmbH, 2019.

Shepherd, A.: Larsen Ice Shelf Has Progressively Thinned, Science, 302, 856–859, https://doi.org/10.1126/science.1089768, http://www.sciencemag.org/cgi/doi/10.1126/science.1089768, 2003.

Shepherd, A., Wingham, D. J., and Mansley, J. A. D.: Inland thinning of the Amundsen Sea sector, West Antarctica: INLAND THINNING OF THE AMUNDSEN SEA, Geophysical Research Letters, 29, 2–1–2–4, https://doi.org/10.1029/2001GL014183, http://doi.wiley.com/10.1029/2001GL014183, 2002.

Spence, P., Griffies, S. M., England, M. H., Hogg, A. M., Saenko, O. A., and Jourdain, N. C.: Rapid subsurface warming and circulation changes of Antarctic coastal waters by poleward shifting winds: Antarctic subsurface ocean warming, Geophysical Research Letters, 41, 4601–4610, https://doi.org/10.1002/2014GL060613, http://doi.wiley.com/10.1002/2014GL060613, 2014.

The IMBIE Team: Mass balance of the Greenland Ice Sheet from 1992 to 2018, Nature, 579, 233–239, https://doi.org/10.1038/s41586-019-1855-2, http://www.nature.com/articles/s41586-019-1855-2, 2020.

Winkelmann, R., Martin, M. A., Haseloff, M., Albrecht, T., Bueler, E., Khroulev, C., and Levermann, A.: The Potsdam Parallel Ice Sheet Model (PISM-PIK) – Part 1: Model description, The Cryosphere, 5, 715–726, https://doi.org/10.5194/tc-5-715-2011, http://www.the-cryosphere.net/5/715/2011/, 2011.

Zhang, T., Price, S. F., Hoffman, M. J., Perego, M., and Asay-Davis, X.: Diagnosing the sensitivity of grounding-line flux to changes in sub-ice-shelf melting, The Cryosphere, 14, 3407–3424, https://doi.org/10.5194/tc-14-3407-2020, https://tc.copernicus.org/articles/14/3407/2020/, 2020.